Acta Crystallographica Section D
Biological Crystallography
ISSN 0907-4449

Structure of tetragonal crystals of human erythrocyte catalase

Martin K. Safo,[a] Faik N. Musayev,[a] Shih-Hsiung Wu,[b] Donald J. Abraham[a] and Tzu-Ping Ko[b]*

[a]Institute for Structural Biology and Drug Discovery, Virginia Commonwealth University, Richmond, VA 23219, USA, and [b]Institute of Biological Chemistry, Academia Sinica, Taipei 11529, Taiwan

Correspondence e-mail: kotping@gate.sinica.edu.tw

Received 22 June 2000
Accepted 4 October 2000

PDB Reference: human erythrocyte catalase, 1f4j.

The structure of catalase from human erythrocytes (HEC) was determined in tetragonal crystals of space group $I4_1$ by molecular-replacement methods, using the orthorhombic crystal structure as a search model. It was then refined in a unit cell of dimensions $a = b = 203.6$ and $c = 144.6$ Å, yielding R and $R_{\rm free}$ of 0.196 and 0.244, respectively, for all data at 2.4 Å resolution. A major difference of the HEC structure in the tetragonal crystal compared with the orthorhombic structure was the omission of a 20-residue N-terminal segment corresponding to the first exon of the human catalase gene. The overall structures were otherwise identical in both crystal forms. The NADPH-binding sites were empty in all four subunits and bound water molecules were observed at the active sites. The structure of the C-terminal segment, which corresponds to the last exon, remained undetermined. The tetragonal crystals showed a pseudo-4_122 symmetry in molecular packing. Two similar types of lattice contact interfaces between the HEC tetramers were observed; they were related by the pseudo-dyad axes.

1. Introduction

Catalase (E.C. 1.11.1.6) catalyzes the conversion of hydrogen peroxide into molecular oxygen and water. It is one of the antioxidant enzymes that protect aerobic organisms from free radicals. Human erythrocyte catalase (HEC) is a tetrameric enzyme of four identical subunits, each containing 527 amino-acid residues, a heme group and an NADPH molecule. The crystal structure of HEC has been determined in an orthorhombic unit cell (Ko *et al.*, 2000; Putnam *et al.*, 2000) and is very similar to the catalase from bovine liver (BLC; Ko *et al.*, 1999). Several other catalases, including the *Saccharomyces cerevisiae* catalase A (SCCA; Maté, Zamocky *et al.*, 1999) and the *Escherichia coli* catalase HPII (Bravo *et al.*, 1999), share a conserved core protein fold, as shown in Fig. 1, although the larger HPII has an additional nucleotide-binding domain.

In the paper by Putnam *et al.* (2000), a detailed analysis of the active-site structure of HEC in complex with several inhibitors was presented. Based on the high-resolution model at 1.5 Å, a mechanism of a 'molecular ruler' for substrate selection was proposed, in which the entry of hydrogen peroxide molecules through the 25 Å long hydrophobic channel to the active site is promoted by a hydrogen-bond network, while the passage of larger molecules is blocked and the access of substrate molecules to the heme iron is controlled by the essential residues His75 and Asn148. In addition to the orthorhombic unit cell, HEC has also been crystallized in monoclinic, tetragonal and hexagonal unit cells (Maté, Ortiz-Lombardia *et al.*, 1999; Ko *et al.*, 2000). The

tetragonal HEC crystals diffracted X-rays to only about 3 Å at room temperature. However, the resolution was subsequently improved to 2.4 Å at cryogenic temperature. This allowed us to proceed with refinement and to compare the HEC structures in different crystal forms.

2. Materials and methods

Purification of HEC from red blood cells, crystallization in the tetragonal unit cell and data collection at room temperature have been described previously (Ko *et al.*, 2000). Some statistics for the diffraction data are presented in Table 1. The crystal structure was solved by molecular-replacement methods using the program *AMoRe* (Navaza, 1994) and the orthorhombic HEC model (PDB code 1qqw). The space group $I4_1$ was determined unambiguously; the asymmetric unit contained an HEC tetramer. The initial model yielded an R of 0.30 and a correlation coefficient of 0.70 for all data within 4.0 Å resolution. Searches with other space groups did not give any solutions. Manual rebuilding and computational refinement employed the programs *O* (Jones *et al.*, 1990) and *CNS* (Brunger *et al.*, 1998) running on an SGI Octane workstation. An 8% subset of randomly selected reflections was reserved to calculate the $R_{\rm free}$ as a monitor of model bias. All data were included whenever an electron-density map was computed.

In the $2F_o - F_c$ difference Fourier map calculated using the 3.0 Å room-temperature data and the model after rigid-body refinement, the N-terminal residues Ser4–Lys23 of all four subunits did not have corresponding density and were actually in severe contact with neighboring molecules. Therefore, the 20 N-terminal residues were omitted. The modified model was used for density modification with fourfold averaging using the program *DM* from the *CCP*4 suite (Collaborative Computational Project, Number 4, 1994). The starting $R_{\rm free}$ and subunit density correlation in *DM* were 0.366 and 0.809–0.820, respectively, which became 0.283 and 0.934–0.937, respectively, at the end. Subsequent refinement employed a single-subunit model and a strict non-crystallographic symmetry (NCS) constraint on the tetramer. The model was adjusted according to the *DM* map and yielded R and $R_{\rm free}$ of 0.258 and 0.341, respectively, after refinement. No significant improvement was seen upon expansion of the model into four NCS-restrained subunits or incorporation of solvent molecules. Moreover, the temperature factors were abnormally low. The refinement could not be completed properly until new data sets were collected at cryogenic temperature using recently upgraded X-ray facilities.

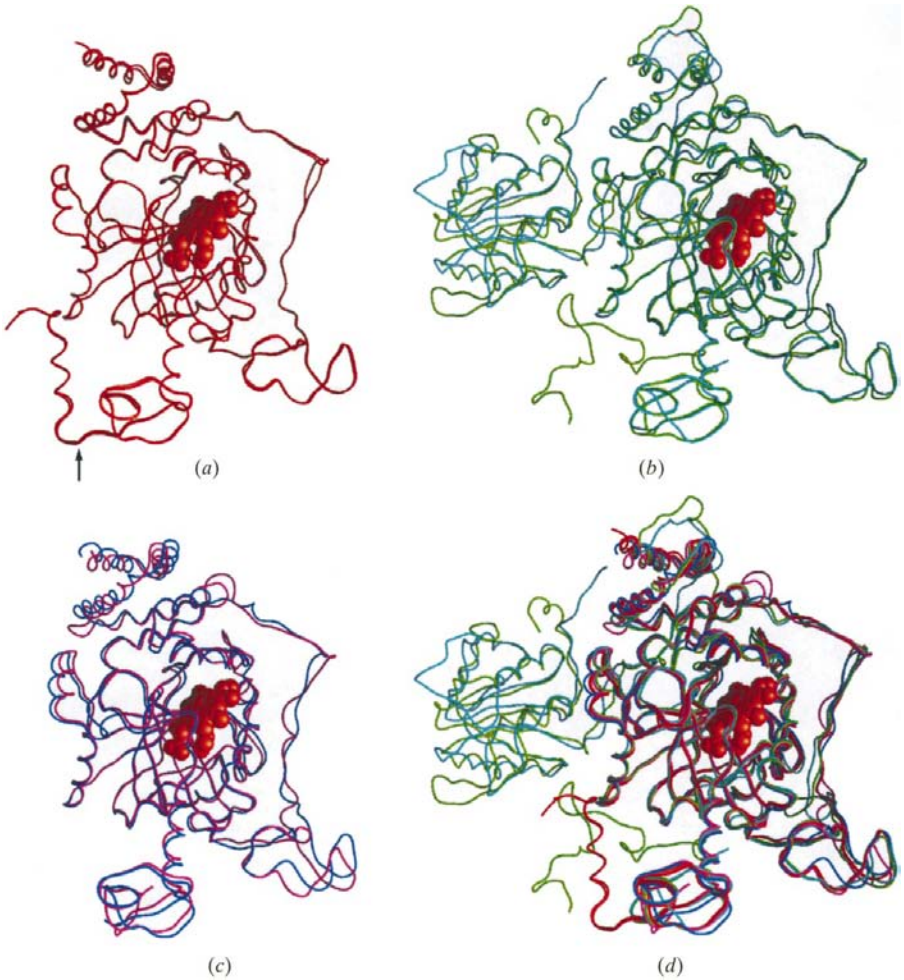

Figure 1
Comparison of catalase structures from different organisms. The subunit models of (*a*) HEC and BLC, shown in orange and red, respectively, (*b*) HPII and PVC, in green and cyan, respectively, (*c*) SCCA and PMC, in magenta and blue, respectively, and (*d*) all six catalases were superimposed by *O* and the protein backbones were drawn using *GRASP*. The heme group is shown in red. NADPH is not shown. The position of Lys23 in HEC is indicated by an arrow in (*a*).

Prior to use in X-ray diffraction, the crystals were washed in a cryoprotectant solution containing 6.25% ethylene glycol, 0.1 *M* HEPES pH 7.5, 1.0 *M* potassium/sodium tartrate and were then transferred to a similar solution containing 12.5% ethylene glycol and finally to another with 25% ethylene glycol. The transfers of the crystals from solution to solution took roughly 1–2 min. Data collection was carried out at 100 K using an MSC X-Stream Cryogenic Crystal Cooler System (Molecular Structure Corporation, The Woodlands, Texas, USA), an R-AXIS II image-plate detector equipped with OSMIC confocal mirrors and a Rigaku RU-200 X-ray generator operating at 50 kV and 100 mA. Data processing employed the *BIOTEX* software (MSC) and the *CCP*4 suite. The effective resolution of the tetragonal HEC crystals was extended from 3 Å to about 2.4 Å under the new experimental conditions, while changes in the unit-cell dimensions were

Table 1
Data-collection statistics.

Values in parentheses refer to the highest resolution shells.

	Crystal 1 (RT)	Crystal 2 (cryo)
Unit-cell parameters (Å)	$a = b = 202.9$, $c = 152.4$	$a = b = 203.6$, $c = 144.6$
Resolution (Å)	122–2.9 (3.0–2.9)	144–2.4 (2.5–2.4)
No. of observations	134056 (10234)	337583 (23586)
Unique reflections	63825 (5739)	107950 (10206)
Average $I/\sigma(I)$	2.67 (1.60)	6.82 (1.66)
Completeness (%)	91.2 (86.0)	92.3 (76.4)
$R_{\rm merge}$ (%)	10.8 (22.3)	6.8 (24.9)

observed. Statistics for the best data set, used in the current refinement, are also listed in Table 1.

The previous model, refined with the 3.0 Å room-temperature data, gave an R value of 0.414 at 2.4 Å for all reflections in the new data set. It was reduced to 0.295 after rigid-body refinement that included a translation of the entire tetramer by about 2 Å and subsequent movements of the four independent subunits. Refinement continued with model adjustments and addition of water molecules according to the difference Fourier maps and cycles of simulated annealing. The criteria for adding water molecules were a density level of more than 1.0σ in the $2F_o - F_c$ map and a distance of less than 6.0 Å from protein atoms. Because there were slight differences in polypeptide conformations of the four subunit models, especially near the crystal contact regions, the NCS restraints were included only in the initial cycles and were released at later stages of refinement. There were also extensions and deletions of a few residues at the termini of the polypeptide chains.

Structure comparison with the orthorhombic crystal was based upon the refined HEC model at 1.5 Å resolution (Putnam *et al.*, 2000; PDB code 1dgf). Other catalase models, including those from *Proteus mirabilis* (PMC; Gouet *et al.*, 1995) and *Penicillium vitale* (PVC; Vainshtein *et al.*, 1981), were also obtained from the Protein Data Bank with reference numbers 4blc (BLC), 1a4e (SCCA), 1cf9 (HPII), 2cae (PMC) and 4cat (PVC). The programs *GRASP* (Nicholls *et al.*, 1991), *MolScript* (Kraulis, 1991), *BobScript* (Esnouf, 1997) and *Raster3D* (Merritt & Murphy, 1994) were used in producing figures.

3. Results and discussion

3.1. Structure refinement and comparison

The final model contained 1918 amino-acid residues, designated *A*24–*A*502, *B*25–*B*503, *C*24–*C*504 and *D*24–*D*502, in four protein subunits, plus four heme groups and 1239 water molecules. NADPH molecules were not included because no density was observed. For all data at 2.4 Å resolution, R and $R_{\rm free}$ were 0.196 and 0.244, respectively. Other refinement statistics are listed in Table 2. The model had very good geometry, with root-mean-square deviations (r.m.s.d.) from ideal bond lengths and angles of 0.0083 Å and 1.45°, respectively. All of the dihedral φ, ψ angles were in the allowed regions of the Ramachandran plot from *PROCHECK* (Laskowski *et al.*, 1993), with the single exception of Ser217. It had the glycine conformation in a tight γ-turn ($\varphi = 70°$, $\psi = -60°$; Richardson, 1981), which was also seen in the orthorhombic crystal of HEC as well as in BLC (Ser216), HPII (Ile274) and SCCA (Gly213). In addition, another non-glycine residue, Asp389, had a special conformation of $\varphi = 60°$, $\psi = -150°$ found in type II′ turns (Richardson, 1981). The peptide Tyr405–Pro406 was in the *cis* configuration. These have also been observed in other catalase structures. The overall coordinate error estimated by a Luzzati plot (Luzzati, 1952) was about 0.31 Å. The r.m.s.d. between model coordinates of the four HEC subunits were 0.22–0.28 Å for the 1912 backbone atoms (N, C^α, C, O), 0.56–0.69 Å for the 1928 side-chain atoms (others) and 0.14–0.22 Å for the 43 heme atoms. If the orthorhombic HEC model was compared, the r.m.s.d.s were 0.32, 1.04 and 0.74 Å for 7644 backbone, 7711 side-chain and 172 heme atoms, respectively. The four heme groups had well defined densities, as shown in Fig. 2. Distances between the heme irons and the bound OH of Tyr358 were 1.93–1.98 Å.

Table 2
Refinement statistics.

Resolution range (Å)	144–2.4 (2.49–2.40)†
No. of reflections	107871 (8603)†
$R_{\rm cryst}$ for 99194 working reflections	0.196 (0.384)†
$R_{\rm free}$ for 8677 test reflections	0.244 (0.406)†
R.m.s.d. from ideal bond lengths (Å)	0.0083
R.m.s.d. from ideal bond angles (°)	1.45
Dihedral angles in most favored regions (%)	85.5
Dihedral angles in additional allowed regions	14.2
Average B values (Å^2)	
16713 non-H atoms	38.1
7672 backbone atoms (N, C^α, C, O)	37.7 (0.69)‡
7734 side-chain atoms (others)	38.2 (1.02)‡
172 heme atoms	37.4
1239 solvent atoms	40.1

† Values for the highest resolution shell. ‡ R.m.s.d. for bonded atoms.

The HEC structures are virtually identical in the orthorhombic and tetragonal crystals, except for the omission of 20 N-terminal residues in the latter. These encompass the helix α1 of the threading arm (Putnam *et al.*, 2000) and correspond to the first exon of the human catalase gene that encodes Met1–Gln22 (Quan *et al.*, 1986). In retrospect, the residues Ala20–Lys23 had weak densities in the maps of the orthorhombic crystal. This region showed high temperature factors in the models of both HEC and BLC. A possible explanation is a break that somehow occurred near Lys23. Thus, the tetragonal HEC model would appear more similar to SCCA, which also has a shorter threading arm (Fig. 1; Maté, Zamocky *et al.*, 1999). Another possible reason for the unobserved N-termini is because of disorder in the crystals. None of the α1 helices were in close contact with neighboring molecules in the orthorhombic crystals of HEC and BLC. However, in the tetragonal crystals the α1 helices of all four subunits must be displaced from the original positions owing to the crystal packing. In either case, the requirement of 4–6 months for crystallization in the tetragonal unit cell can be explained by slow rearrangement of the threading arm or slow dissociation

of the α-helix from the subunit surface. On the other hand, residues Glu503 and Lys504 were seen as an extension of the C-terminal helix. The peptide conformation beyond this point, including the 21-residue segment Asn507–Leu527 encoded by the last exon, was not determined. Neither has a corresponding polypeptide segment at the C-terminus been observed in BLC or SCCA. Regardless of the questionable N- and C-termini, the redissolved tetragonal crystals showed a full level of enzymatic activity compared with the commercial BLC and freshly prepared HEC samples (Musayev, Safo & Abraham, unpublished data). It would be intriguing to investigate the biological function of the first and last exons of the human catalase gene.

The Matthews coefficient or specific volume (Matthews, 1968) of the tetragonal HEC crystals was 3.1 Å^3 Da^{-1}, corresponding to a high solvent content of about 60%. Of the 1239 water molecules in the model of the tetragonal crystal, 640 had equivalents in the orthorhombic crystal, with distances of less than 1.0 Å upon superposition. While 277 of these water molecules were located on the tetramer surface, 363 were buried in the protein, including those in the central cavity and the solvent channels; 248 were found in the inter-subunit interfaces, but only 28 were near the inter-tetramer interfaces. No water molecule was bound directly to the heme iron at the active site. However, in two subunits there were two water molecules bound to each other and to the NE and ND2 of His75 and Asn148, respectively; in the other two subunits there was only one water molecule bound to His75. Similar active-site water molecules were also observed in the orthorhombic HEC crystals and were found in the structures of SCCA and HPII as well. The empty NADPH-binding sites remained essentially unchanged from the search model, in which all four subunits had the side chains of Phe198 in the 'A' conformation (Ko *et al.*, 2000). It is now clear that binding of NADPH will switch the side chain of Phe198 to the 'B' conformation (Putnam *et al.*, 2000). Previous ambiguity in the orthorhombic BLC crystals (Ko *et al.*, 1999) was probably caused by partial occupancies.

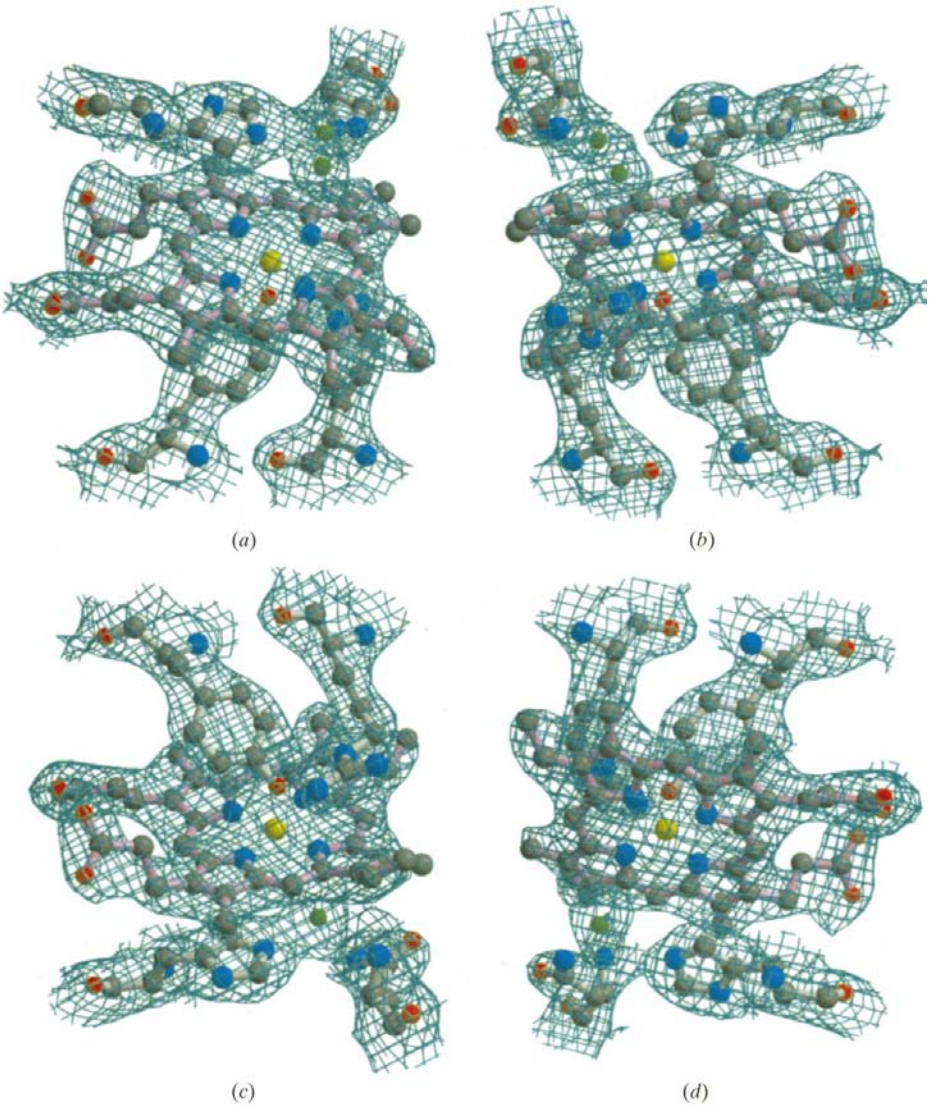

Figure 2
Difference Fourier ($2F_o - F_c$) maps of the four heme groups in the tetragonal HEC crystal. Maps were calculated using the final model and contoured at 1.0σ level, colored cyan. The heme groups of subunits *A*, *B*, *C* and *D* are shown in (*a*), (*b*), (*c*) and (*d*), respectively, with bonds in pink. Also shown are the residues His75, Asn148, Arg354 and Tyr358, as well as one or two active-site water molecules, colored green. The figures were produced using *BobScript* and *Raster3D*.

3.2. Crystal packing and lattice interactions

Fig. 3 shows molecular-packing diagrams of the tetragonal HEC crystal. Each tetramer (*e.g.* the one labelled 0 in Fig. 3) is in contact with four symmetry-related neighbors, two (labelled 1 and 1′) by the 4_1 screw axis and two others (labelled 2 and 2′) by the 4_3 axis. In other words, there are two types of crystal contact interfaces. Not taking water molecules into account, the first and second types of interfaces between molecules related by the 4_1 and 4_3 symmetry involved at least 42 and 35 amino-acid residues, respectively. Specific bonds are listed in Table 3. When the bonds in interfaces I and II were compared, five out of nine bonds were identical, although the distances were slightly different, and equivalent residues were involved in the remaining four bonds. If bonds mediated by water molecules were also included, the residues involved in the two intermolecular contact regions would become virtually identical. Interface I buried 951 Å^2 surface area on one molecule and 986 Å^2 on

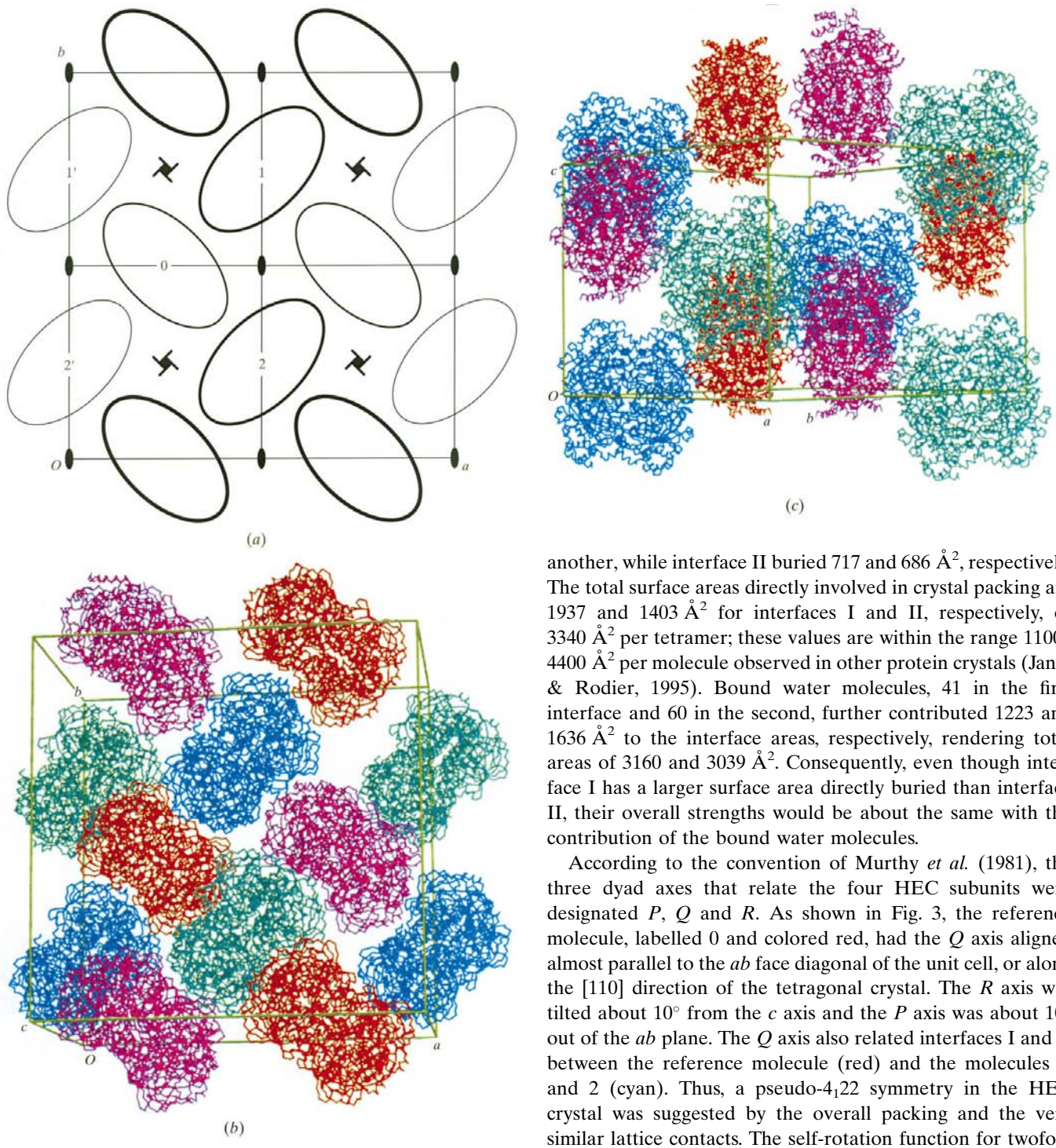

Figure 3
A schematic packing diagram (*a*) and two views of HEC tetramers in the $I4_1$ crystal (*b* and *c*). In (*a*) the view is along the *c* axis, with the *a* and *b* axes pointing to the right and top. Molecules are shown as ovals. Those at the front are denoted by thick lines. Locations of the crystallographic dyad axes and the 4_1 and 4_3 screw axes are also indicated. In (*b*) and (*c*) the tetragonal unit cell is shown in green. Molecules related by the 4_1 symmetry are shown in cyan, red, blue and magenta, and molecules related by the body-centered lattice symmetry in the same colors. In (*b*) the view is similar to (*a*). In (*c*) the view is along the diagonal, in the $[1\bar{1}0]$ direction, with the *a* and *b* axes pointing to the right and the *c* axis to the top. Some molecules were omitted for clarity. The figure was produced using *Molscript* and *Raster3D*. See text for explanation regarding the labels 0, 1, 2, 1′ and 2′.

another, while interface II buried 717 and 686 Å^2, respectively. The total surface areas directly involved in crystal packing are 1937 and 1403 Å^2 for interfaces I and II, respectively, or 3340 Å^2 per tetramer; these values are within the range 1100–4400 Å^2 per molecule observed in other protein crystals (Janin & Rodier, 1995). Bound water molecules, 41 in the first interface and 60 in the second, further contributed 1223 and 1636 Å^2 to the interface areas, respectively, rendering total areas of 3160 and 3039 Å^2. Consequently, even though interface I has a larger surface area directly buried than interface II, their overall strengths would be about the same with the contribution of the bound water molecules.

According to the convention of Murthy *et al.* (1981), the three dyad axes that relate the four HEC subunits were designated *P*, *Q* and *R*. As shown in Fig. 3, the reference molecule, labelled 0 and colored red, had the *Q* axis aligned almost parallel to the *ab* face diagonal of the unit cell, or along the [110] direction of the tetragonal crystal. The *R* axis was tilted about 10° from the *c* axis and the *P* axis was about 10° out of the *ab* plane. The *Q* axis also related interfaces I and II between the reference molecule (red) and the molecules 1′ and 2 (cyan). Thus, a pseudo-4_122 symmetry in the HEC crystal was suggested by the overall packing and the very similar lattice contacts. The self-rotation function for twofold symmetry showed peaks perpendicular to the *c* axis with 45° intervals and 3–5° from the *a* axis. A typical plot is shown in Fig. 4. The peak heights of the pseudo-dyad symmetry were approximately 80% of the crystallographic symmetry along the *c* axis. The pseudo-4_122 symmetry in the arrangement of tetramers was partially expressed in the diffraction patterns of the crystal, with an approximate 4*mm* symmetry in the *hk*0 zone. However, when the data were processed with 422 symmetry, we observed an $R_{\rm sym}$ of about 32%, which is much higher than the $R_{\rm sym}$ for 4 symmetry of about 9%. Therefore, the true space group should be $I4_1$.

Variations in the unit-cell volumes were observed upon flash-cooling of crystals to cryogenic temperature. For example, the flash-frozen monoclinic crystal of HPII was reduced in unit-cell volume by 3.8% with respect to the crystal at room temperature (Bravo *et al.*, 1999). Likewise, the second tetragonal HEC crystal used in this refinement was reduced in unit-cell volume by 4.5% with respect to the first crystal. One possibility for the reduction was because of dehydration. This is probably the case with the monoclinic HPII crystals, in which all three axial dimensions of the unit cell were reduced by similar fractions. For the tetragonal HEC crystals the mechanism might be different. The shrinking of the unit cell was not proportional. Specifically, the reduction of unit-cell volume was principally contributed by an approximately 5% reduction in the *c*-axis dimension, while there was almost no change in the *a* and *b* axes. In our diffraction experiments at cryogenic temperature, another HEC crystal had unit-cell parameters $a = b = 203.0$, $c = 147.3$ Å. It seems likely that the HEC molecules can be disposed in the tetragonal unit cell with a number of variations in the length of the *c* axis from crystal to crystal. It is shown in Fig. 3 that the HEC molecules had a spiral arrangement with contacts between neighbors related by the 4_1 and 4_3 screw axes only. No other type of intermolecular contact was observed. Although the two interfaces I and II are almost identical, there could be slight variations, especially in the second interface, which involved more bonds mediated by water molecules. These would lead to a significant change in the length of the *c* axis.

In the tetragonal and orthorhombic crystals, the HEC molecules had completely different arrangements. They were packed with different lattice interfaces that involved different sets of surface residues. However, comparison of the contact residues in Table 3 of this paper (tetragonal form) and Table 2 of Ko *et al.* (2000) (orthorhombic form) showed that the interfaces involved two common residues, Arg*A*47 (*C*47) and Pro*A*106 (*C*106). Besides, as noted in the previous section, 28 equivalent water molecules were near the packing interfaces. Fig. 5 shows the interface areas of both crystal forms on the HEC molecule. Apparently, portions of the interfaces cover adjacent areas, but the two areas of interface I in the orthorhombic crystal (colored red) are actually related separately to

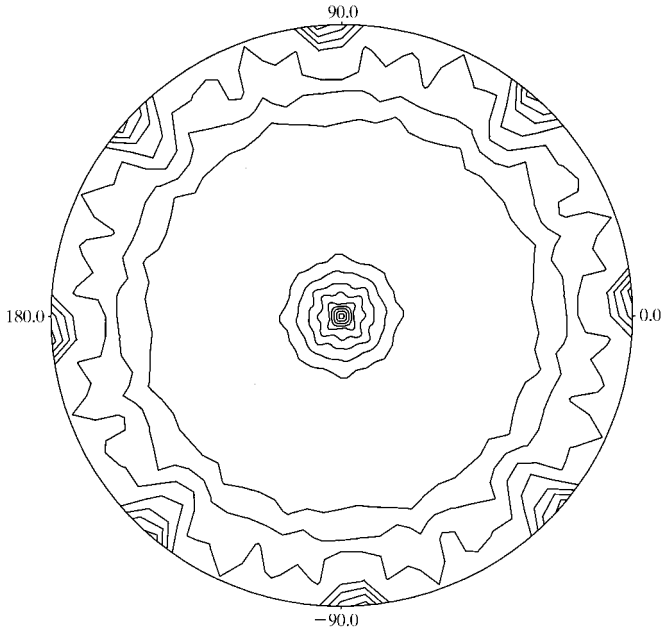

Figure 4
A self-rotation function plot with $\kappa = 180^\circ$ for dyad symmetry. The view of the spherical map is along the *c* axis, while the locations of the *a* and *b* axes are indicated by the labels $\varphi = 0$ and 90°. The plot was generated using the program *POLARRFN* from the *CCP*4 suite. The radius and resolution range were 28 and 8–2.5 Å, respectively.

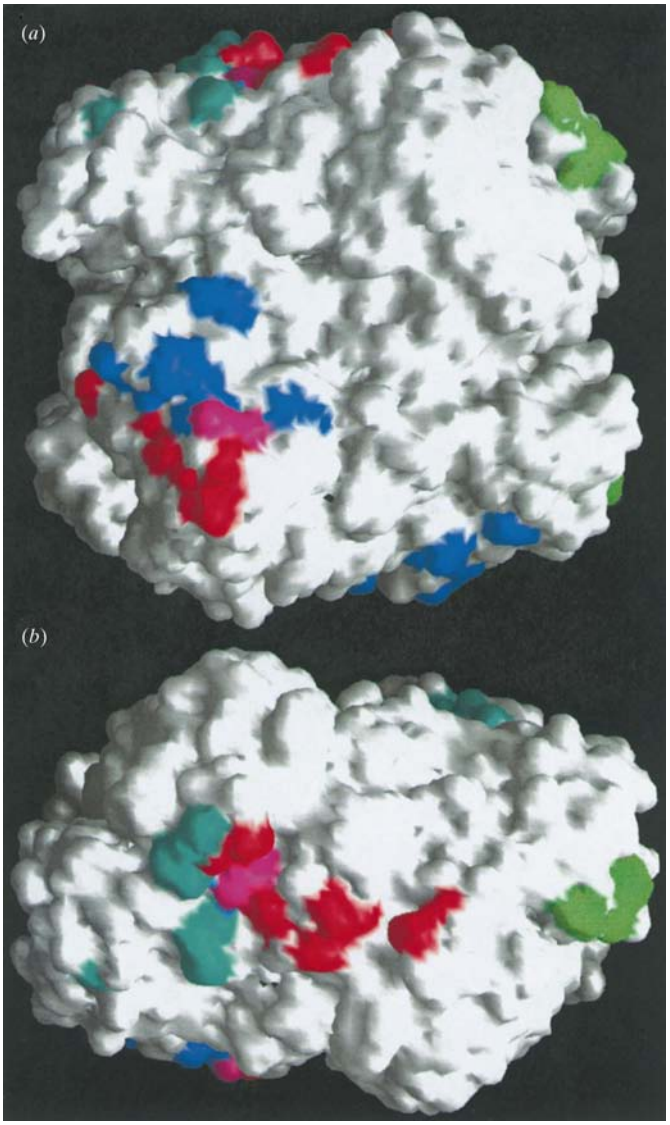

Figure 5
Contact interfaces of the HEC molecule. (*a*) and (*b*) are two orthogonal views with a horizontal rotation of 90°. The residues directly involved in crystal packing interactions are mapped onto the surface of an HEC tetramer. Areas of interfaces I and II in the orthorhombic crystal are shown in red and green, respectively, and areas of interfaces I and II in the tetragonal crystals in blue and cyan, respectively. Each interface is comprised of two distinct surface patches that are contributed by two opposing HEC molecules. The locations of Arg*A*47 and Pro*A*106 are shown in magenta.

Table 3
Residues directly involved in crystal contacts.

(*a*) Interface I, for molecules related by (1) x, y, z and (2) $1 - y, \frac{1}{2} + x, \frac{1}{4} + z$.

Residue 1 atom	Residue 2 atom	*d* (Å)	Comments
Tyr*B*84 OH	Asn*D*436 OD1	2.87	Hydrogen bond
Ala*B*270 O	Arg*A*47 NH1	3.15	Hydrogen bond
Tyr*B*274 OH	Arg*A*47 NH2	3.11	Hydrogen bond
Tyr*B*274 OH	Asp*D*437 OD2	2.83	Hydrogen bond
Asn*B*319 ND2	Asn*D*436 O	3.11	Hydrogen bond
Val*B*323 CG2	Pro*D*293 CG	3.19	VDW contact
Arg*B*380 NH2	Thr*D*483 O	2.98	Hydrogen bond
Gln*C*173 OE1	Thr*D*291 OG1	3.25	Hydrogen bond
Gln*C*173 NE2	Thr*D*291 O	2.89	Hydrogen bond

(*b*) Interface II, for molecules related by (1) x, y, z and (2) $y, \frac{1}{2} - x, \frac{1}{4} + z$.

Residue 1 atom	Residue 2 atom	*d* (Å)	Comments
Thr*B*291 O	Gln*D*173 NE2	2.95	Hydrogen bond
Pro*B*293 CG	Val*A*323 CG2	3.39	VDW contact
Ser*B*426 OG	Lys*A*273 NZ	3.45	Hydrogen bond
Asn*B*436 ND2	Tyr*A*84 OH	3.17	Hydrogen bond
Asn*B*436 OD1	Lys*A*106 NZ	3.10	Hydrogen bond
Asn*B*436 O	Asn*A*319 ND2	3.37	Hydrogen bond
Glu*B*484 OE1	Arg*A*380 NE	2.85	Salt bridge
Glu*B*484 OE2	Arg*A*380 NH2	3.01	Salt bridge
Arg*C*47 NH2	Tyr*A*274 OH	3.11	Hydrogen bond

areas of different interfaces I and II in the tetragonal crystal (blue and cyan). Thus, the two common residues (in magenta) belong to different interfaces. The 28 equivalent water molecules were not a result of conserved lattice interactions; presumably they were associated with individual protein surfaces.

This work was supported by the National Institutes of Health (Grant HL-32793).

References

Bravo, J., Maté, M. J., Schneider, T., Switala, J., Wilson, K., Loewen, P. C. & Fita, I. (1999). *Proteins*, **34**, 155–166.

Brunger, A. T., Adams, P. D., Clore, G. M., Delano, W. L., Gros, P., Grosse-Kunstleve, R. W., Jiang, J. S., Kuszewski, J., Nilges, M., Pannu, N. S., Read, R. J., Rice, L. M., Simonson, T. & Warren, G. L. (1998). *Acta Cryst.* D**54**, 905–921.

Collaborative Computational Project, Number 4 (1994). *Acta Cryst.* D**50**, 760–763.

Esnouf, R. M. (1997). *J. Mol. Graph.* **15**, 132–134.

Gouet, P., Jouve, H. M. & Dideberg, O. (1995). *J. Mol. Biol.* **249**, 933–954.

Janin, J. & Rodier, F. (1995). *Proteins*, **23**, 580–587.

Jones, T. A., Zou, J. Y., Cowan, S. W. & Kjeldgaard, M. (1990). *Acta Cryst.* A**47**, 110–119.

Ko, T.-P., Day, J., Malkin, J. & McPherson, A. (1999). *Acta Cryst.* D**55**, 1383–1394.

Ko, T.-P., Safo, M. K., Musayev, F. N., Martino, L. D. S., Wang, C., Wu, S.-H. & Abraham, D. J. (2000). *Acta Cryst.* D**56**, 241–245.

Kraulis, P. J. (1991). *J. Appl. Cryst.* **24**, 946–950.

Laskowski, R. A., MacArthur, M. W., Moss, D. S. & Thornton, J. M. (1993). *J. Appl. Cryst.* **26**, 283–291.

Luzzati, P. V. (1952). *Acta Cryst.* **5**, 802–810.

Maté, M. J., Ortiz-Lombardia, M., Marina, A. & Fita, I. (1999). *Acta Cryst.* D**55**, 1066–1069.

Maté, M. J., Zamocky, M., Nykyri, L. M., Herzog, C., Alzari, P. M., Betzel, C., Koller, F. & Fita, I. (1999). *J. Mol. Biol.* **286**, 135–149.

Matthews, B. W. (1968). *J. Mol. Biol.* **33**, 491–497.

Merritt, E. A. & Murphy, M. E. P. (1994). *Acta Cryst.* D**50**, 869–873.

Murthy, M. R. N., Reid, T. J., Sicignano, A., Tanaka, N. & Rossmann, M. G. (1981). *J. Mol. Biol.* **152**, 465–499.

Navaza, J. (1994). *Acta Cryst.* A**50**, 157–163.

Nicholls, A., Sharp, K. A. & Honig, B. (1991). *Proteins*, **11**, 281–296.

Putnam, C. D., Arvai, A. S., Bourne, Y. & Tainer, J. A. (2000). *J. Mol. Biol.* **296**, 295–309.

Quan, F., Korenluk, R. G., Tropak, M. B. & Gravel, R. A. (1986). *Nucleic Acids Res.* **14**, 5321–5335.

Richardson, J. S. (1981). *Adv. Protein Chem.* **34**, 167–339.

Vainshtein, B. K., Melik-Adamyan, W. R., Barynin, V., Vagin, A. A. & Grebenko, A. I. (1981). *Nature (London)*, **293**, 411–412.